Research Square

Preprints are preliminary reports that have not undergone peer review.
They should not be considered conclusive, used to inform clinical practice,
or referenced by the media as validated information.

Suppression-induced fuel accumulation can amplify extreme fire seasons in Iberia

Francesca Di Giuseppe

francesca.digiuseppe@ecmwf.int

European Centre for Medium-range Weather Forecasts

Adrian Mark Tompkins

UNESCO-ICTP

Joe McNorton

European Centre for Medium-range Weather Forecasts

Article

Keywords:

Posted Date: October 29th, 2026

DOI: https://doi.org/10.21203/rs.3.rs-11365106/v1

License: This work is licensed under a Creative Commons Attribution 4.0 International License.
Read Full License

Additional Declarations: No competing interests reported.

Suppression-induced fuel accumulation can amplify extreme fire seasons in Iberia

Francesca Di Giuseppe[1*], Adrian Mark Tompkins[2] and Joe McNorton[1]

[1]European Centre for Medium-range Weather Forecasts, Shinfield Park, Reading, RG2 9AX, United Kingdom.
[2]UNESCO-ICTP, Strada Costiera 11, Trieste, 34151, Italy.

*Corresponding author(s). E-mail(s): francesca.digiuseppe@ecmwf.int;

Abstract

Recent extreme fire seasons in Europe highlight the need to understand what drives this escalation and how fuel accumulation, weather variability and suppression interact to shape it. We analyse May–October burned area across mainland Iberia during 2003–2025 and identify a bimodal distribution, with ordinary seasons separated from four extreme years exceeding 4,000 km^2. Seasonal totals in these extreme years are dominated by a small number of large, spatially clustered fire events, motivating an examination of how extreme seasons emerge when suppression capacity is exceeded. A conceptual stochastic model combining fuel accumulation, weather variability and suppression reproduces this bimodal structure, with suppression acting as a perturbation to the balance between fuel accumulation and fire-driven fuel removal. Storyline simulations indicate that strong suppression produces low-fire seasons but allows fuel to accumulate, setting the stage for occasional extreme seasons when containment capacity is exceeded. In a scenario with doubled fuel accumulation, potentially associated with landscape abandonment and greater fuel continuity, the simulated frequency of high-fire seasons increases from 12% to 36%, while the 90th percentile of seasonal burned area rises from 4,684 to 10,092 km^2. Stronger suppression can substantially reduces the frequency of high-fire seasons but has a smaller effect on their severity. These results indicate that fuel accumulation, reinforced by strong suppression practices, shapes extreme fire regimes. Fuel management and suppression must therefore be considered together to limit both the occurrence and severity of extreme fire seasons.

Keywords: Mediterranean wildfire; burned area; large fires; fuel availability; fire suppression; nonlinear dynamics

1 Introduction

Fire regimes across the Iberian Peninsula are marked by strong contrasts between relatively quiet years and exceptional seasons, with regional burned area varying by more than an order of magnitude and, in our 2003–2025 record, by a factor of approximately 37 between the lowest- and highest-burned-area years [1–3]. During these high-fire years, large and rapidly spreading fires can occur simultaneously, challenging suppression capacity across the region [4–7].

Anthropogenic warming is increasing the likelihood of dangerous fire weather across Mediterranean Europe through more intense heat, atmospheric dryness and drought [2, 5, 8, 9], which increased winter and spring precipitaton increase fuel accumulation rate [10]. However, this increase has not produced widespread positive trends in burned area or fire emissions. Indeed, annual burned area has declined across much of Mediterranean Europe in recent decades, although important regional exceptions remain, partly reflecting changes in land use and management, prevention interventions and improved fire suppression capacity [11–13]. Fire weather defines the conditions under which fire can spread, while the area that actually burns also depends on the biophysical and human controls that operate within those conditions.

This distinction is particularly important for extreme seasons. A small fraction of very large fires accounts for a disproportionate share of total burned area in Mediterranean Europe [1, 3]. The occurrence of extreme fire events depends on the joint effects of fuel abundance, fuel dryness, weather, landscape connectivity and suppression [1, 12, 14]. When fire growth exceeds containment capacity, burned area can increase rapidly, while simultaneous incidents can further limit containment by competing for finite suppression resources [4, 6, 7].

Unlike weather, which varies over days to seasons, fuel availability carries a memory of previous years. Across Mediterranean Europe, agricultural abandonment, afforestation and a decline in grazing have transformed heterogeneous agricultural landscapes into more continuous areas of shrubland and forest [1, 12, 15, 16]. These changes increase fuel abundance and connectivity over years to decades. When drought and extreme fire weather dry the accumulated vegetation, a greater proportion of this biomass becomes available to sustain fire growth [2, 14].

Suppression is connected to this longer-term fuel balance. Extinguishing fires reduces burned area, but consequently also retains vegetation that would have been consumed. Thus suppression without land management can lead to fuel accumulation, and leave a larger share of burning associated with severe conditions under which containment is less effective [12, 17]. Fuel accumulation and suppression may therefore influence one another rather than acting as independent controls on fire activity.

These interactions provide a mechanism through which distinct low- and high-fire seasons could emerge. In most years, fire growth may remain within the range that suppression can contain. Occasionally, abundant and sufficiently dry fuel may allow fire activity to grow faster than suppression can contain, producing a season with much greater burned area. Such behavior could produce a long upper tail or multiple peaks in the distribution of seasonal burned-area totals [18, 19]. If high-fire seasons also contain exceptionally large burned patches, this would indicate that they differ

from ordinary seasons not only in total area, but also in the spatial scale of individual events within the season [3].

Here, we use May–October burned-area observations from 2003–2025 to examine these patterns across mainland Iberia. We first test whether high-fire seasons form a distinct statistical group and whether their exceptional totals arise from a few very large, connected burned patches. We then use a stochastic conceptual model of self-organised criticality to reproduce the observed inter-annual variability in Iberia and examine how it emerges from the feedback between fuel accumulation and suppression strength. Using this conceptual model, we explore how changes in fuel accumulation and suppression strength, individually and together, affect the frequency and magnitude of extreme fire seasons. Although calibrated for Iberia, the framework may also apply to other regions where suppression contains most fires but occasional escaped fires dominate regional burned area. Together, these analyses address a central question of how do fuel, fire and suppression interact to generate extreme fire seasons, and how does the system respond when fuel accumulation, suppression strength or both change.

2 Results

2.1 Fire-season two-mode regime across mainland Iberia

We analyze May–October burned area across mainland Iberia from 2003–2025 using the MODIS Collection 6.1 burned-area product (MCD64A1; [20]), aggregated from its native 500-m resolution to a 9-km grid [21, 22]. The product maps the spatial extent of burned surfaces from changes in MODIS surface reflectance, providing an observation of realised burned area rather than fire occurrence or activity. Satellite detection can be affected by cloud cover, dense vegetation, small or short-duration burns, and limitations in temporal sampling. We therefore also assess agreement with independent national burned-area statistics (Methods), which show good consistency with the satellite-derived estimates in terms of annual totals (Supplementary material). To examine the spatial organisation of burning, we group connected burned cells into annual patches and retain those larger than 10 km^2 (Methods). These patches are connected components of observed burned area and do not necessarily correspond one-to-one with individual fire perimeters. Instead, they describe the spatial scale and concentration of realized burning within each season.

Regional burned area ranges from 178 km^2 in 2008 to 6,592 km^2 in 2003. Seasonal totals separate into a lower mode containing most years and an upper mode comprising 2003, 2005, 2017 and 2025 (Fig. 1b). These four seasons record 6,592, 4,774, 6,381 and 6,342 km^2 of burned area, respectively, and all exceed the 4,176 km^2 intersection between the two fitted components. A two-component distribution provides a better description of the MODIS annual totals than a single Gaussian distribution (Methods; Supplementary S3 S2 and S3).

This separation is also evident in independent EFFIS country statistics [23], which provide a substantially longer record for Spain and Portugal. Over the overlapping period, the relative ordering of seasons is broadly consistent between datasets: 2003 and 2017 are among the years with the greatest burned area, whereas 2008 and 2018

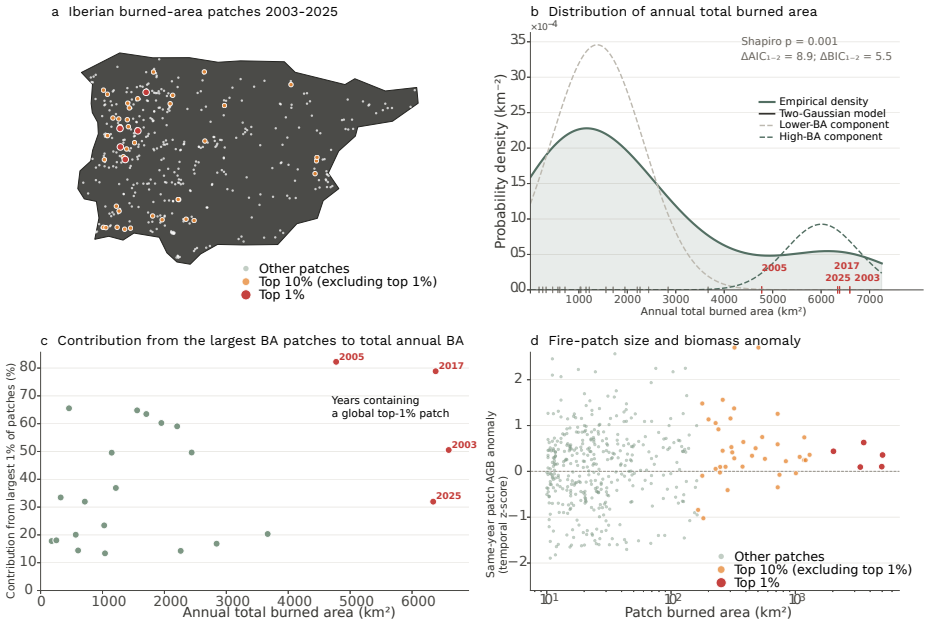


Fig. 1 Annual burned area and its spatial organization across mainland Iberia, 2003–2025. a, Connected burned-area patches larger than 10 km^2. Colors distinguish patches in the largest 1% of the complete catalog, patches in the remainder of the largest 10%, and all other retained patches. **b**, Distribution of annual May–October burned area calculated from all raster cells, including patches smaller than 10 km^2. Years containing at least one patch from the largest 1% of the complete catalog are marked in red. Lines show the empirical density, the fitted two-component Gaussian mixture and its two components. **c**, Percentage of each year's total burned area contributed by the largest 1% of patches selected independently within that year. **d**, Same-year above-ground biomass (AGB) anomaly collocated with each burned patch as a function of patch area. Colours follow panel **a**.

are among the lowest. Despite differences in spatial coverage, observation method and seasonal definition, the national statistics show the same broad contrast between predominantly low-burned-area years and a smaller number of exceptionally large fire seasons. Analysis of the full national record further supports the presence of this structure beyond the MODIS period (Supplementary Material).

We interpret the observed distribution as an empirical two-mode structure in realized annual burned area. Given the relatively short 23-year satellite record, however, we do not interpret the separation as evidence of an irreversible temporal regime shift. The upper mode is not only characterized by large annual totals it also coincides with the appearance of exceptionally large connected burned-area patches. In 2005 and 2017, the largest 1% of patches within each year account for 82% and 79% of the total, respectively. The corresponding contributions are 51% in 2003 and 32% in 2025 (Fig. 1c). These four high-fire-mode seasons therefore differ in the spatial distribution of fire activity, indicating that the distinction between high- and low-fire modes reflects not only the amount of burning but also its spatial concentration. This concentration of regional burned area within a small number of exceptionally large patches

is consistent with fire-size distributions reported elsewhere in Mediterranean Europe [1, 3, 24].

A large fractional contribution from the largest patches is not, by itself, sufficient to place a season in the upper mode. In 2018, for example, the largest 1% of patches account for 66% of the annual total, but only 459 km^2 burned across the study region. High-fire seasons therefore occur when the dominant patches are sufficiently large, or sufficiently numerous, to raise the regional total above the range occupied by ordinary years. The upper mode is associated primarily with the absolute scale of these patches rather than their percentage contribution alone.

The co-occurrence of high annual totals and exceptionally large patches indicates a regional pattern of burning that extends beyond the spatial scale normally observed during lower-mode seasons. We refer to this pattern as "escaped" burning, while recognizing that the fire clusters may connect separate fires that burn adjacent areas at different times and provide no direct information on the suppression of individual fires. Evidence from individual Iberian fires nevertheless shows that warming preferentially enhances the spread of the most rapidly growing fires, while simultaneous incidents can place additional pressure on suppression capacity [2, 6].

We finally examine whether the largest connected patches occur in anomalous vegetation conditions by collocating each patch with its same-year above-ground biomass (AGB) anomaly (Fig. 1d) using a fuel characteristic model. The model combines satellite-derived AGB estimates from the ESA Climate Change Initiative (CCI) Biomass product [25] with modeled carbon fluxes informed by atmospheric CO_2 inversions to represent temporal changes in vegetation biomass [26]. The largest patches coincide with positive AGB anomalies, indicating that the most extensive patches occur where above-ground vegetation is more abundant than usual. This relationship is descriptive and does not establish that greater anomalous AGB causes larger burned patches. AGB represents the amount of standing above-ground vegetation and is therefore an indicator of potential fuel abundance, rather than a direct measurement of fuel available to burn. It does not distinguish live from dead vegetation or describe fuel moisture. Drought and extreme fire weather determine how much of this biomass becomes sufficiently dry to sustain fire [2, 3, 27]. The observed association therefore supports a role for vegetation abundance in the largest burned patches, while we acknowledge that fuel dryness, fire weather and suppression are also critical factors.

3 A fuel–fire–suppression mechanism for two fire-season states

Annual burned area separates into two groups, with the most extreme seasons dominated by exceptionally large burned patches. This motivates a dynamical interpretation in which fire activity emerges from interactions between fuel availability, weather variability and suppression.

We represent these interactions using a stochastic conceptual model with three state variables: fire activity (F), available fuel (V) and a delayed suppression response (R; Methods). The model belongs to the Lotka–Volterra family [28, 29] and draws on self-organised descriptions of fire regimes [18, 19, 30, 31].

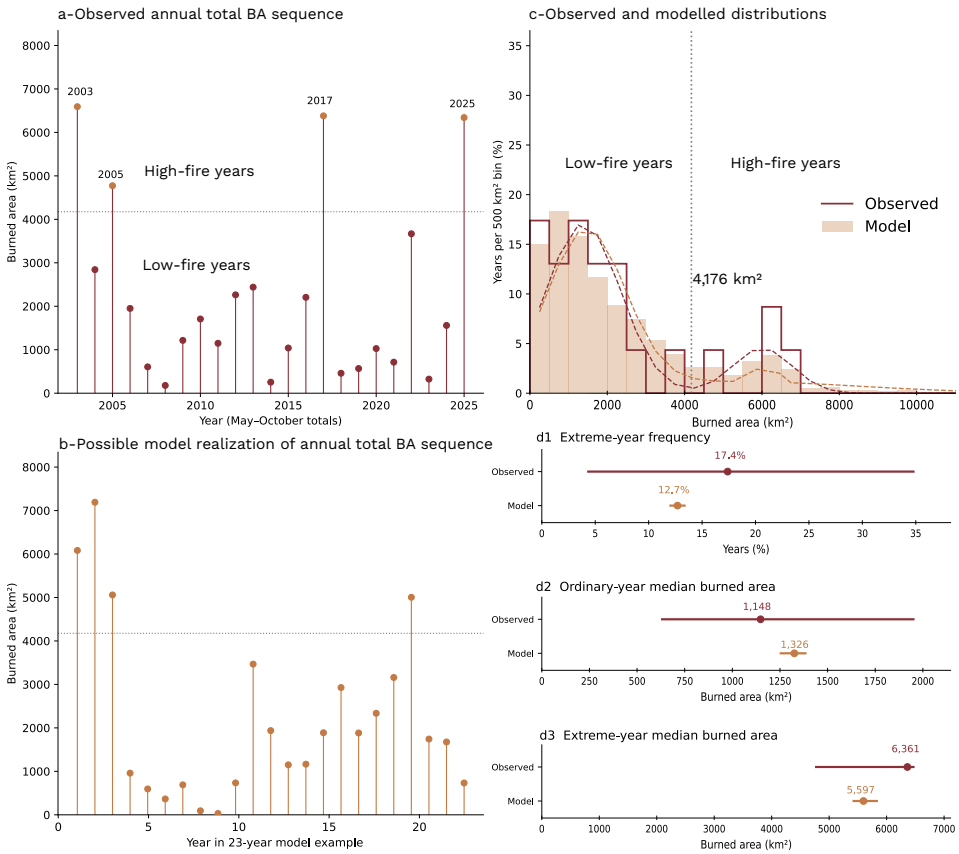


Fig. 2 Observed and modeled annual burned-area distributions across mainland Iberia. **a**, Observed May–October burned area from 2003–2025. The dotted line marks the empirical 4,176 km^2 boundary between low- and high-fire years (Methods). **b**, A representative 23-year realization of the calibrated stochastic model, illustrating the occurrence of occasional high-fire seasons. **c**, Observed and modeled burned-area distributions. Lines show the estimated densities, and bars show the percentage of years within each 500 km^2 interval. **d**, Comparison of three distributional characteristics: (**d1**) frequency of high-fire years, (**d2**) median burned area during low-fire years and (**d3**) median burned area during high-fire years. Points show the observed and modeled estimates, and horizontal lines show their 95% uncertainty intervals (Methods). Model estimates are obtained from independent stochastic simulations using the calibrated parameter set.

Ignitions initiate fire activity in the model, but they do not determine the final burned area. Fire grows when sufficient fuel is available, while stochastic weather variability modulates its rate of spread. Suppression responds to increasing fire activity by removing fires from the system, with a probability of success that depends on the level of suppression effort and weather severity. Fires that escape suppression continue to consume fuel, while vegetation growth gradually replenishes the available fuel. The resulting burned area therefore emerges from the balance between fuel-supported fire growth and the capacity of suppression to contain ongoing fire activity.

The model represents fire activity over an idealized fraction of a regional domain rather than simulating individual fires explicitly. At any given time, fire activity, fuel availability and suppression interact dynamically, and under stable forcing the system tends towards a natural balance in which fire growth is offset by fuel consumption and suppression.

When fire activity grows slowly enough for suppression to keep pace, this balance is reached at relatively low levels of burning and the seasonal total falls within the low-fire group. When abundant fuel and favorable weather allow fire activity to grow faster than suppression can respond, the system is temporarily displaced from this equilibrium. Burning then continues until fuel depletion and the delayed suppression response reduce fire activity and restore balance. These episodes generate much larger seasonal totals and form the extreme burnt area mode.

The model does not predict the size of individual fires. Instead, by integrating the simulated fraction of the domain affected by fire over the days of a season, it provides an estimate of the total fraction, and, after scaling by the regional area, the total area—experiencing fire during that season.

We calibrate the model against the observed burned-area distribution to test whether this mechanism reproduces the main statistical features of Iberian fire seasons (Fig. 2). The observed record contains mostly low-fire years, interrupted by four high-fire seasons above the empirical boundary of 4,176 km^2 (Fig. 2a). A representative 23-year model realisation shows a similar alternation between common low-fire years and occasional high-fire years (Fig. 2b). Across independent simulations, the model reproduces the overall shape and two-group structure of the observed distribution (Fig. 2c).

The model also captures the frequency and characteristic magnitude of the two groups. High-fire years occur in 12.7% of modeled seasons, compared with 17.4% of the observed record. Median burned area during low-fire years is 1,326 km^2 in the model and 1,148 km^2 in the observations. During high-fire years, the corresponding medians are 5,597 and 6,361 km^2, respectively (Fig. 2d1–d3). The model therefore reproduces both the predominance of relatively limited fire seasons and the occasional emergence of seasons with substantially greater burned area.

3.1 Fuel accumulation amplifies extreme fire seasons

Having established that the self-organised fire model captures the main features of the observed distribution, we use it to examine how fire seasons respond to changes in fuel accumulation and suppression. Increasing winter and spring precipitation could contribute to an increase in fuel accumulation in future climates, while drier, warmer summers can also contribute both to fuel quality in the appropriate and the frequency of sustained fire ignitions which can then grow. We do not attempt to explicitly model the impact of climate change on fuel availability, but instead we adopt a storyline approach to show how different combinations of fuel availability and suppression strength affect the frequency and magnitude of high-fire seasons.

Greater fuel accumulation strongly increases both how frequent the high fire years can return and how large those fire years could be (Fig. 3). Fixing the suppression rate to the value calibrated for the contemporary period, halving fuel accumulation reduces

the frequency of high-fire years from 12.0% to 1.9% and lowers the outcome of the most intense years (90th percentile of annual burned area) from 4,684 to 2,283 km^2. Doubling fuel accumulation increases the frequency to 36% and raises the 90th percentile to 10,092 km^2. When increasing the fuel accumulation rate by a factor of 4, 58% of simulated seasons enter the high-fire group and the 90th percentile reaches 21,566 km^2 (Fig. 3a,c,d).

The response to changes in suppression is less direct. At the present-day fuel-accumulation rate, 12.0% of years fall into the high-fire mode under reference suppression, compared with 11.3% when suppression is halved and 8.5% when it is doubled. Increasing suppression to four times the reference strength reduces this frequency further, to 7.1%. This relatively weak and non-linear response reflects two opposing processes in the model. Stronger suppression limits fire activity within individual seasons, but by preventing burning it also allows more vegetation to remain available as fuel in subsequent years. This effect on fuel availability is substantial: doubling suppression approximately doubles mean available fuel, while increasing suppression fourfold raises it to about 3.7 times the reference level (Fig. 3b,e).

The interaction between suppression and fuel accumulation becomes more pronounced under high-fuel conditions. At four times the present-day fuel-accumulation rate, increasing suppression from its reference strength to four times that level reduces the frequency of high-fire years from 57.4% to 19.2%. In contrast, the magnitude of the most severe seasons changes much less: the 90th percentile of annual burned area decreases by only 9%, from 21,566 to 19,653 km^2. In the model, stronger suppression therefore substantially reduces the frequency with which high-fire seasons occur, but has a smaller effect on their magnitude once abundant fuel allows fire activity to escape containment.

This behavior is consistent with the wildfire suppression paradox [17, 32], which states that suppressing fires reduces burning in the short term but retains fuel that can support future extreme events. In Iberia, agricultural abandonment, declining grazing and vegetation recovery may contribute to this longer-term accumulation. The model does not represent these processes separately, however, and instead combines their effects within a single fuel-accumulation parameter.

To test whether the Iberian behavior is specific to the regional calibration or reflected a more general property of the model structure, we repeated the analysis for Greece using the same fire–fuel–suppression equations and recalibrating only the effective fuel-replenishment and suppression parameters. Greece provides a useful contrast because its observed annual burned-area distribution is predominantly single-peaked rather than showing the two-group structure identified in Iberia. Despite this difference, the same model framework reproduces the Greek distribution with an effective fuel-replenishment parameter almost identical to Iberia ($G/G_{\mathrm{Iberia}} = 1.01$) but a lower effective suppression parameter ($c/c_{\mathrm{Iberia}} = 0.72$). This contrast supports the interpretation that the Iberian two-group structure is not imposed by the model equations themselves, but emerges from the interaction between fuel replenishment and suppression strength (Supplementary material and Figure S3)

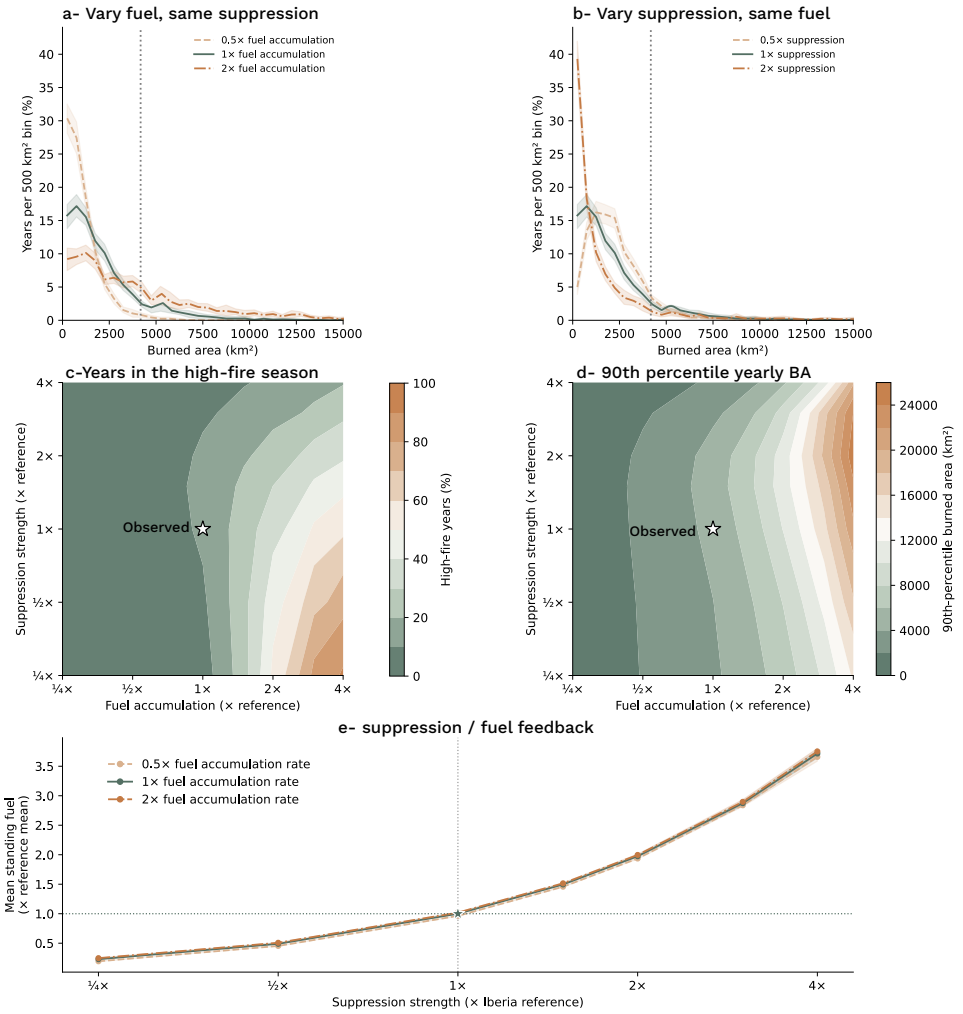


Fig. 3 Sensitivity of fire seasons to fuel accumulation and suppression. a, Distribution of annual burned area under different fuel-accumulation rates and reference suppression. **b**, Distribution of annual burned area under different suppression strengths and reference fuel accumulation. The vertical dotted line in **a,b** marks the observed 4,176 km^2 boundary between low- and high-fire years. **c**, Percentage of simulated years in the high-fire group across combinations of fuel accumulation and suppression strength. **d**, Corresponding 90th percentile of annual burned area. **e**, Mean retained fuel with increasing suppression strength, expressed relative to the reference simulation and shown for three fuel-accumulation rates. The star marks the calibrated Iberian reference conditions. Shaded bands show 95% uncertainty intervals from the stochastic simulations. All multipliers are expressed relative to the calibrated Iberian values.

4 Discussion

Our results suggest that extreme fire seasons in Iberia emerge from the interaction between fuel availability and suppression, with high-fire years associated with exceptionally large, connected burned patches. The model indicates that fuel accumulation is a key control on the severity and frequency of these seasons, consistent with the broader concern that agricultural abandonment, declining grazing, forest expansion and reduced fire activity can increase both vegetation abundance and fuel continuity across Mediterranean landscapes [12, 33, 34]. Once sufficiently dry, this accumulated biomass can sustain fire spread over much larger areas, reinforcing the need to consider longer-term fuel dynamics alongside suppression.

Suppression in Iberia has a more complex influence because it affects both current burning and the fuel available for subsequent seasons. In the short term, stronger suppression limits fire activity, particularly during small and moderate events. Over longer periods, however, vegetation that would otherwise have burned remains in the landscape. In our simulations, doubling suppression approximately doubles mean available fuel, while a fourfold increase raises it to about 3.7 times the reference level. This feedback is consistent with the paradox of wildfire suppression, in which successful fire exclusion reduces burning immediately but can contribute to conditions that support more severe fires later [17, 32].

This result does not imply that suppression is ineffective. Suppression remains essential for protecting lives, infrastructure and ecosystems, and the simulations show that it can substantially reduce the frequency of high-fire seasons. Its influence on their severity becomes more limited, however, when fuel is abundant. At four times the reference fuel accumulation, increasing suppression fourfold reduces the frequency of high-fire years from 57.4% to 19.2%, but lowers the 90th percentile of annual burned area by only about 9%, from 21,566 to 19,653 km^2. Stronger suppression therefore prevents many high-fire seasons, but the fires that escape containment can still generate relative extreme regional totals.

Fuel management and suppression should consequently not be treated as alternative or independent strategies. Suppression provides immediate protection, whereas fuel management modifies the conditions under which future fires spread and suppression operates. Prescribed burning, grazing, mechanical treatment and other locally appropriate measures can reduce fuel abundance or disrupt its continuity, potentially widening the range of conditions under which fires remain containable. These longer-term interventions should be combined with prevention, preparedness, and strong response capacity [1, 12]. Their appropriate balance will vary among landscapes and must account for ecological objectives, smoke exposure, carbon storage and operational constraints.

The main contribution of this study is to connect patterns that are commonly examined at different scales. We relate the distribution of seasonal burned area to the concentration of burning in exceptionally large patches and then use a stochastic dynamical model to examine how theoretical fuel availability and suppression can generate this distribution. Although deliberately simple, the model reproduces the observed separation between ordinary and extreme seasons and allows fuel accumulation and suppression to be varied together. The simulations reveal that the processes

controlling the frequency of high-fire seasons are not necessarily the same as those controlling their magnitude. Suppression can greatly reduce how often these seasons occur, while accumulated fuel continues to influence the severity of those that escape containment, here understood as the set of mechanisms capable of extinguishing fires.

This framework may also be useful in other regions where strong suppression keeps most fires small but occasional escaped fires dominate regional burned area (see more in supplementary information). Similar trade-offs may arise where afforestation, forest expansion, vegetation recovery or other land-use changes increase biomass and fuel continuity. Although these processes can provide important carbon and ecological benefits, their consequences for fire depend on the type, moisture, spatial arrangement and management of the additional fuel [35]. Because G is an effective parameter representing the net rate of fuel accumulation, the model can explore sensitivity to such changes but cannot distinguish the contributions of climate, CO_2 fertilisation or specific land-management practices. Recalibrating the model against regional observations could reveal how the balance between fuel accumulation and suppression differs among fire regimes. Such comparisons would require independent information on vegetation dynamics, fire weather, management and suppression systems before the model parameters could be given a direct physical or operational interpretation.

Several limitations remain. The observational record contains only 23 fire seasons, although the broad separation between ordinary and exceptional years is consistently supported by independent country-level burned-area statistics and complementary diagnostics (Methods; Supplementary Material). Connected burned patches do not necessarily correspond to individual fire events. The model does not explicitly represent spatial fuel patterns, individual suppression resources, changing ignition pressure or particular fuel-management practices. Weather variability is represented stochastically rather than using observed or projected meteorological conditions. The storylines experiments should therefore be interpreted as sensitivities of the conceptual system, not as forecasts of particular future seasons. Within these limits, the consistency between the observed structure, independent metrics and modeled distributions supports a central interpretation: extreme Iberian fire seasons become more likely when accumulated fuel allows fire growth to outpace suppression, and managing this risk requires attention to both sides of that interaction.

5 Methods

5.1 Data

5.2 Burned-area observations and independent verification

The study covers mainland Spain, Portugal and Andorra, with a total area of 595,717 km^2. We analyses May–October burned area from 2003 to 2025 using the MODIS Collection 6.1 burned-area product (MCD64A1; [20]), aggregated from its native 500-m resolution to a 9-km grid [21, 22]. Burned-area values are converted to square kilometers before analysis.

The study-domain mask is constructed by intersecting the burned-area grid with the mainland boundaries of Spain, Portugal and Andorra. A grid cell is included when

its centre falls within the study domain. The resulting mask contains 12,799 cells and remains unchanged throughout the analysis.

For each year, the six monthly BA fields from May to October are summed before any patch-size threshold is applied. Seasonal burned area is then calculated as the sum of all positive burned-area values within the regional mask. All six months are available for each of the 23 seasons, and missing cell values are retained as missing rather than interpreted as zero burned area.

We assess the consistency of the raster-derived regional series against independent annual country statistics collected by EFFIS [23]. The national series is constructed by summing the reported annual burned area for Spain and Portugal. The common compariso period is 2003–2024, comprising 22 paired years; the MODIS series extends to 2025, whereas the national record used here extends from 1980 to 2024.

The two datasets are not expected to agree in absolute magnitude. The MODIS analysis represents May–October burning over mainland Iberia, whereas the national statistics represent complete calendar years and national territories. They also differ in observation method, spatial definition, minimum mapped-fire size and treatment of land-cover classes. We therefore use the comparison to evaluate consistency in inter-annual variability and the relative ordering of high- and low-fire years, rather than equality of absolute burned-area estimates.

Across the 22 common years, the two records are strongly correlated (Pearson $r = 0.979$; Spearman $r = 0.967$). The national totals are, on average, higher than the raster estimates, with a mean difference of 434 km^2 and an aggregate national-to-raster ratio of 1.22. These systematic differences are consistent with the contrasting seasonal and geographical definitions of the two datasets and are not interpreted as measurement bias. Full agreement statistics and bootstrap confidence intervals are reported in Supplementary material.

5.3 Identification and robustness of the two-component structure in seasonal burned area

We characterize the distribution of annual burned area using Gaussian mixture models fitted to the seasonal totals in raw km^2. One- and two-component Gaussian models are fitted using identical preprocessing and compared using the Akaike and Bayesian information criteria (AIC and BIC). Positive values of ΔAIC and ΔBIC, defined as the information criterion of the single-Gaussian model minus that of the two-Gaussian model, therefore favor the two-component representation. For the two-component model, we additionally verify that the fitted probability density contains two distinct maxima and calculate the intersection between the component densities as a descriptive boundary between lower- and upper-component seasons.

The analysis is first applied independently to the MODIS and national records over their common 2003–2024 period, and is then repeated using the complete MODIS record (2003–2025) and the full national record (1980–2024). This design tests whether the inferred distributional structure depends on a particular observational product or period. Classification agreement between the two sources is evaluated only over their common years, with each source using parameters estimated from its own distribution; the MODIS-derived threshold is not imposed on the national statistics.

Normality is assessed separately using the Shapiro–Wilk, D'Agostino K^2, Jarque–Bera and Anderson–Darling tests. These tests are used only to assess the adequacy of a Gaussian description and are not interpreted as tests of unimodality. Because the observational records are short and extreme years can strongly affect mixture-model fitting, robustness is further assessed using contiguous 22-year windows of the national record, random subsamples of equivalent length, component effective sample sizes and alternative single-peaked distributions.

These analyses distinguish evidence for a reproducible two-component representation from stronger claims of statistically unique bimodality. Accordingly, throughout the study we refer to an empirical two-mode or two-group structure. Full distributional diagnostics and sensitivity tests are reported in the Supplementary Material.

5.3.1 Connected burned-area patches

We use connected components to characterize the spatial organization of burning within each season. Positive cells in the accumulated May–October raster are grouped using eight-neighbor connectivity, which treats cells sharing either an edge or a corner as connected. Patch area is calculated as the sum of the burned-area values of all cells belonging to the same component. We retain patches with an area of at least 10 km^2.

These components describe contiguous areas of observed burning within the accumulated seasonal raster. They are not interpreted as individual fire perimeters because adjacent areas burned by separate fires, or during different months, can form a single annual patch.

For Fig. 1a,d, we rank all retained patches from 2003–2025 together and identify the largest 10% and 1% of the complete catalogue. For Fig. 1c, patches are ranked independently within each year. If a year contains N_y retained patches, we sum the areas of the largest $\lceil 0.01 N_y \rceil$ patches and divide this sum by the total raster-derived burned area for that year. The denominator includes all observed burned area, including burning belonging to patches smaller than 10 km^2.

5.3.2 Above-ground biomass

We use annual above-ground biomass (AGB) from [26] at a spatial resolution of **9 km**. The data combines satellite-derived AGB estimates from the ESA Climate Change Initiative (CCI) Biomass product [25] with modelled carbon fluxes informed by atmospheric CO_2 inversions to represent temporal changes in vegetation biomass [26]. AGB is converted from kg m^{-2} to Mg ha^{-1} where required and collocated with the burned-area grid using bilinear interpolation.

For each year and grid cell, we calculate an AGB anomaly relative to that cell's temporal mean and standard deviation over the whole 2003-2025 period:

$$Z_{i,y} = \frac{\mathrm{AGB}_{i,y} - \overline{\mathrm{AGB}} * i}{\sigma * \mathrm{AGB}, i}, \tag{1}$$

where $Z_{i,y}$ is the standardized anomaly in cell i and year y. The anomaly therefore describes whether the amount of standing vegetation in a cell is greater or smaller than usual for that location.

Patch-level anomalies are calculated as the area-weighted mean of the cell anomalies belonging to each 10% of its area has valid AGB observations. Missing values are otherwise excluded from the patch mean.

We compare AGB anomalies among the largest 1% of patches, the remainder of the largest 10%, and all other retained patches, and examine the association between AGB anomaly and patch area. Because AGB measures standing above-ground vegetation rather than directly burnable fuel, this analysis is interpreted as a descriptive test of the association between patch size and vegetation abundance, rather than as evidence that high AGB alone causes extensive burning.

5.4 Modeling

5.4.1 Fuel–fire–suppression model

We use a stochastic Lotka–Volterra-type model [28, 29] to represent interactions among fire activity, available fuel and suppression. The model contains three normalized state variables: the instantaneous burned-area rate (F), available fuel (V) and suppression response (R). It is intended as a minimal representation of their interactions rather than a reconstruction of individual fires or firefighting operations. At each time step, the model represents the fraction of a hypothetical domain that is actively burning, the fraction of vegetation that remains available as fuel, and the corresponding suppression response. Fire activity can be amplified by stochastic weather variability, which is treated as an external forcing, and reduced by suppression, whose strength is prescribed as a controllable model parameter. Integrating the burned-area rate through time gives the total fraction of the domain burned over the simulated season, which is then converted to regional burned area.

The burned-area rate evolves according to

$$\frac{dF}{dt} = \widetilde{w}(t)VF(1-F) + I(t) - cR, \tag{2}$$

where $\widetilde{w}(t)$ represents stochastic weather variability, $I(t)$ represents ignition forcing and c controls suppression strength. The interaction VF allows existing fire activity to grow when fuel is available, while $(1-F)$ limits this growth as F approaches its normalized upper bound.

Weather variability follows an Ornstein–Uhlenbeck process with a decorrelation timescale of 2.5 days. The Gaussian process is transformed through its cumulative distribution function to a Weibull distribution with shape parameter 2 and unit mean [36–38]. This produces persistent, positively skewed fluctuations in the environmental conditions affecting fire growth. Because the stochastic forcing varies around a unit mean, weather can act in either direction: values above the mean represent periods favorable to fire growth, whereas values below the mean represent less favorable conditions that constrain fire activity. The weather term should therefore not be interpreted as a particular meteorological index, but as a conceptual representation of short-timescale variability in the combined atmospheric conditions influencing fire spread and intensity. Unlike fuel accumulation and suppression strength, which are varied

systematically in the experiments, the weather sequence is treated as an external stochastic forcing over which the model has no control.

Ignition opportunities occur independently at a constant mean probability of 0.003 per day. When an ignition occurs and $F < 0.05$, a forcing of 10^{-4} is applied for one integration step. Ignition probability and magnitude remain constant during calibration and all scenario experiments. The model therefore isolates changes arising from fuel replenishment and suppression rather than changes in ignition pressure.

Suppression responds to established fire activity with a finite delay:

$$\frac{dR}{dt} = \rho[F - I(t) - R] \tag{3}$$

where ρ controls the rate at which suppression approaches fire activity after excluding the instantaneous ignition forcing. We set $\rho = 1$ day^{-1}, corresponding to a characteristic response timescale of one day. Here, suppression is represented conceptually as the capacity to remove active fire from the system once burning is established. It therefore encompasses any process that contributes to extinguishing or containing fire, rather than representing a specific firefighting resource or operational strategy. Suppression strength is treated as a controllable model parameter, in contrast to the stochastic weather forcing, which acts externally on fire growth. As fire activity increases, the suppression response strengthens, but because the response is delayed it may fail to keep pace when fire growth becomes sufficiently rapid.

Available fuel evolves according to

$$\frac{dV}{dt} = G(1 - V) - \beta F \tag{4}$$

where G controls fuel replenishment and β controls consumption by fire. We set $\beta = 0.3$. The normalized variable V represents the combined influence of fuel abundance, continuity and availability. In real landscapes, these properties can be modified by multiple processes, including vegetation growth and mortality, drought and fuel drying, land-use and vegetation change, previous fire activity and fuel-management practices. The conceptual model does not distinguish among these individual mechanisms; rather, they are represented collectively through changes in fuel availability and replenishment. Its purpose is therefore not to attribute changes in burned area to a specific fuel process, but to examine how changes in the overall fuel state interact with fire activity and suppression to determine regional burned area.

For small F, negligible instantaneous ignition and a suppression response close to $R \approx F$, the growth condition can be approximated by

$$\widetilde{w}(t)V < c \tag{5}$$

Fire activity tends to decline under this condition. When $\widetilde{w}(t)V$ exceeds c, activity can grow faster than suppression responds until fuel consumption and the delayed response restore control. This inequality is used only to interpret the model mechanism and is not imposed as an explicit threshold during integration.

We integrate Eqs. 2–4 using a fourth-order Runge–Kutta scheme with a time step of 0.05 days. After each integration step, F and R are constrained to remain non-negative and V is constrained to lie between zero and one. Simulations begin from $F = 0$, $V = 0.2$ and $R = 0$.

Each 365-day model interval represents one complete fire-system cycle rather than a reconstruction of a particular calendar year. The full-year integration allows fuel replenishment, fire activity and suppression to evolve continuously across successive cycles, including periods outside the observed May–October fire season. This is important because the model is designed to represent interannual fuel carry-over and feedbacks between burning, vegetation availability and suppression; restricting the model itself to the observational season would interrupt these dynamics.

Weather forcing is stochastic, so an individual simulation represents only one possible realization of the fire system for a given combination of fuel and suppression parameters. We therefore perform a large ensemble of independent realizations for each parameter combination and analyse the resulting distribution of annual burned-area outcomes. The ensemble is used to characterize not only the central tendency of the system, but also the frequency and magnitude of rare high-fire seasons.

The modelled burned-area fraction in cycle y is calculated as

$$b_y = \int_y F(t)\, dt \tag{6}$$

where F is interpreted as the instantaneous fraction of the study domain burned per day. Modeled burned area is then

$$B_y = b_y A_{\text{Iberia}}, \tag{7}$$

where $A_{\text{Iberia}} = 595,717\ \text{km}^2$.

For each parameter combination, we summarize the simulated distribution using two complementary diagnostics. The fraction of simulated cycles assigned to the high-fire mode quantifies how frequently extreme seasons occur, whereas the 90th percentile of annual burned area quantifies the magnitude of the upper tail. The 90th percentile is the burned-area value exceeded by only 10% of simulated cycles and is therefore used here as a measure of the scale of the most severe seasons generated by the model.

The observational record is restricted to May–October, while the model is integrated over complete 365-day cycles. The two are therefore compared at the level of their burned-area distributions rather than as matched calendar periods or year-by-year reconstructions. The 365-day model cycle should be interpreted as the natural integration period of the conceptual system, whereas the May–October observational window defines the empirical distribution against which the model behaviour is evaluated.

5.4.2 Model calibration and evaluation

We calibrate fuel replenishment (G) and suppression strength (c) jointly against the complete observed distribution of Iberian seasonal burned-area fractions. The search is conducted in logarithmic parameter space over

$$G \in [3.525 \times 10^{-7},\ 1.128 \times 10^{-5}] \tag{8}$$

and

$$c \in [0.00575,\ 0.092]. \tag{9}$$

These bounds span 0.25–8 times the initial reference value of $G = 1.41 \times 10^{-6}$ and 0.25–4 times the initial reference value of $c = 0.023$. They were chosen to explore a broad range of fuel-replenishment and suppression regimes around the parameter values used during model development while avoiding parameter values approaching zero. All remaining model parameters are held fixed.

We use differential evolution as implemented in `scipy.optimize.differential_evolution`, with a population-size multiplier of six and a maximum of 32 iterations. The optimisation is performed with a relative convergence tolerance of 0.005, an absolute tolerance of 0.001, no final polishing step, and a fixed optimiser random seed of 701. The mutation range and recombination coefficient are left at their SciPy defaults, $(0.5, 1.0)$ and 0.7, respectively. The search is initialised at

$$G = 1.4114 \times 10^{-6}, \qquad c = 0.02315.$$

Each proposed parameter pair is evaluated using two independent stochastic simulations with seeds 42 and 2026. Each simulation contains 1,000 model years, of which the first 500 are discarded as spin-up, leaving 500 retained years per realization.

Agreement between the observed and simulated distributions is measured using the first-order Wasserstein distance in linear burned-area-fraction space:

$$J(G, c) = \frac{W_1(b_{\mathrm{obs}}, b_{\mathrm{sim}}(G, c))}{\bar{b}_{\mathrm{obs}}}, \tag{10}$$

where b_{obs} is the observed distribution of annual burned-area fractions, $b_{\mathrm{sim}}(G, c)$ is the simulated distribution for a given parameter pair, and $\bar{b}_{\mathrm{obs}}$ is the mean observed burned-area fraction. The objective is calculated separately for the two stochastic realizations and their normalized Wasserstein distances are then averaged. A single parameter pair is therefore calibrated against the complete observed distribution; the low- and high-fire groups are not fitted separately.

The optimisation gives

$$G_0 = 3.1282 \times 10^{-6}, \qquad c_0 = 0.04324. \tag{11}$$

We evaluate this parameter pair using four additional stochastic seeds (111, 222, 333 and 444) that are not used during calibration. Each evaluation contains 2,000 model years, of which the first 500 are discarded as spin-up, providing 6,000 retained annual values in total. Model performance is summarized by the percentage of retained years above the observed 4,176 km^2 boundary and by the median burned areas below and above that boundary.

Finite-simulation uncertainty is estimated using 300 circular moving-block bootstrap samples with a block length of 20 model years. Blocks are sampled with replacement to produce a resample equal in length to the simulated series, and 95% intervals are defined by the 2.5th and 97.5th percentiles. These intervals describe

stochastic sampling uncertainty conditional on the calibrated values (G_0, c_0). They do not include uncertainty in the calibrated parameters or uncertainty arising from the limited observational record.

5.4.3 Fuel-accumulation and suppression experiments

Starting from the calibrated reference values (G_0, c_0), we vary fuel replenishment and suppression strength factorially by

$$0.25, ; 0.5, ; 1, ; 1.5, ; 2, ; 3 \quad \text{and} \quad 4 \tag{12}$$

times their respective reference values. Stochastic weather characteristics, ignition probability, ignition magnitude, suppression-response time, fuel consumption and all other model parameters remain unchanged.

For each combination, we run two independent simulations of 3,000 model years and discard the first 1,500 years of each simulation as spin-up. We combine the retained values and calculate the distribution of annual burned area, the percentage of model years above the observed 4,176 km^2 boundary, the 90th percentile of annual burned area and mean retained fuel. Mean retained fuel is calculated as the temporal mean of V and expressed relative to the value obtained under (G_0, c_0).

Uncertainty is estimated using 300 circular moving-block bootstrap samples with a block length of 20 model years. These intervals represent stochastic variability conditional on each parameter combination and do not include uncertainty in G_0 or c_0.

The experiments describe the sensitivity of the conceptual system to theoretical changes in fuel replenishment and suppression. They are not dated projections. Translating climatic change, agricultural abandonment, vegetation management or operational suppression policies into particular changes in G and c would require additional observations or external models.

Acknowledgements. We acknowledge funding from the ESA Open Calls programme under the FUELITY project (ESA contract 4000144712/24/I-DT-bgh).

Funding. ESA Open Calls programme under the FUELITY project (ESA contract 4000144712/24/I-DT-bgh).

Conflict of interest. The authors declare no conflict of interest.

Data availability. The MODIS/Terra+Aqua MCD64A1 Collection 6.1 burned-area product is openly available from the NASA Land Processes Distributed Active Archive Center (LP DAAC) through NASA Earthdata. The product provides monthly 500-m burned-area maps with a burn-date layer identifying the day of year on which each burned pixel was detected. The data are available at https://doi.org/10.5067/MODIS/MCD64A1.061 . Fuel-characteristic data are available at https://doi.org/10.24381/378d1497. Figure data will be released with the analysis workflow upon publication.

Code availability. Analysis and figure workflows will be archived on Zenodo (https://doi.org/10.5281/zenodo.6572507).

Author contributions. FDG conceived the study, performed the primary analysis, and led the writing. AMT developed the mathematical and numerical framework for the self organized model. JM contributed to the data curation and data analysis. All authors revised the manuscript.

References

[1] Fernandes, P.M., Barros, A.M., Pinto, A., Santos, J.A.: Characteristics and controls of extremely large wildfires in the western mediterranean basin. Journal of Geophysical Research: Biogeosciences **121**(8), 2141–2157 (2016)

[2] Senande-Rivera, M., Insua-Costa, D., Miguez-Macho, G.: Climate change aggravated wildfire behaviour in the Iberian Peninsula in recent years. npj Climate and Atmospheric Science **8**, 19 (2025) https://doi.org/10.1038/s41612-025-00906-3

[3] Ghasemiazma, F., Tonini, M., Fiorucci, P., Turco, M.: Megafires in Mediterranean Europe: the compound role of fire weather and drought. npj Natural Hazards **3**, 33 (2026) https://doi.org/10.1038/s44304-026-00197-5

[4] Fernandes, P.M., Pacheco, A.P., Almeida, R., Claro, J.: The role of fire-suppression force in limiting the spread of extremely large forest fires in portugal. European Journal of Forest Research **135**(2), 253–262 (2016)

[5] Ruffault, J., Curt, T., Martin-StPaul, N.K., Moron, V., Trigo, R.M.: Increased likelihood of heat-induced large wildfires in the Mediterranean Basin. Scientific Reports **10**, 13790 (2020) https://doi.org/10.1038/s41598-020-70069-z

[6] Torres-Vázquez, M.Á., Di Giuseppe, F., Moreno-Torreira, A., Gincheva, A., Jerez, S., Turco, M.: Large increase in extreme fire weather synchronicity over Europe. Environmental Research Letters **20**(2), 024045 (2025) https://doi.org/10.1088/1748-9326/ada8c2

[7] Sánchez-Hernández, G., Turco, M., Repeto-Deudero, I., Royé, D., Baudena, M., Montávez, J.P., Pietroiusti, R., Provenzale, A., Santin, C., Torres-Vázquez, M.Á., *et al.*: Record-breaking 2025 european wildfires concentrated in northwest iberia. Global Change Biology **31**(12), 70649 (2025)

[8] Barbero, R., Abatzoglou, J.T., Pimont, F., Ruffault, J., Curt, T.: Attributing increases in fire weather to anthropogenic climate change over France. Frontiers in Earth Science **8**, 104 (2020) https://doi.org/10.3389/feart.2020.00104

[9] El Garroussi, S., Di Giuseppe, F., Barnard, C., Wetterhall, F.: Europe faces up to tenfold increase in extreme fires in a warming climate. npj Climate and Atmospheric Science **7**(1), 30 (2024)

[10] Burton, C., Di Giuseppe, F., Jones, M.W., Kelley, D.I., Barbosa, M.L.F., McNorton, J., Potts, R., Segura-Garcia, C., Abatzoglou, J.T., Alin Rosu, I., Andela,

N., Anderson, L.O., Archibald, S., Brambleby, E., Chuvieco, E., Ciavarella, A., Clarke, H., Barrera, F., Di Bella, C.M., Di Tomaso, E., Dintwe, K., Doherty, T.S., Donovan, V.M., Eden, J.M., Fernandes, P.M., Fiedler, L., Giglio, L., Haas, O., Hamilton, D., Hantson, S., Harris, S., Hartley, A.J., Keeping, T.R., Kolden, C.A., Kouassi, J.-L., Kukavskaya, E., Lampe, S., Liu, Z., Mataveli, G., Meier, S., Oom, D., Parrington, M., Qu, Y., Dios, V., Ruffault, J., Sadegh, M., Santín, C., Sedano, F., Shuman, J.K., Silva, P.S., Spuler, F.R., Steinmann, C.B., Tanpipat, V., Torres-Vazquez, M.A., Turco, M., Werf, G.R., Wees, D., Veraverbeke, S., Wessel, J.B., Zheng, B.: State of wildfires 2025–2026. Earth System Science Data Discussions **2026**, 1–111 (2026) https://doi.org/10.5194/essd-2026-587

[11] Turco, M., Bedia, J., Di Liberto, F., Fiorucci, P., Hardenberg, J., Koutsias, N., Llasat, M.C., Xystrakis, F., Provenzale, A.: Decreasing fires in Mediterranean Europe. PLOS ONE **11**(3), 0150663 (2016) https://doi.org/10.1371/journal.pone.0150663

[12] Moreira, F., Ascoli, D., Safford, H., Adams, M.A., Moreno, J.M., Pereira, J.M., Catry, F.X., Armesto, J., Bond, W., González, M.E., *et al.*: Wildfire management in mediterranean-type regions: paradigm change needed. Environmental Research Letters **15**(1), 011001 (2020)

[13] Carnicer, J., Alegria, A., Giannakopoulos, C., Di Giuseppe, F., Karali, A., Koutsias, N., Lionello, P., Parrington, M., Vitolo, C.: Global warming is shifting the relationships between fire weather and realized fire-induced co2 emissions in europe. Scientific reports **12**(1), 10365 (2022)

[14] Ruffault, J., Curt, T., Martin-StPaul, N.K., Moron, V., Trigo, R.M.: Extreme wildfire events are linked to global-change-type droughts in the northern Mediterranean. Natural Hazards and Earth System Sciences **18**, 847–856 (2018) https://doi.org/10.5194/nhess-18-847-2018

[15] Pausas, J.G., Fernández-Muñoz, S.: Fire regime changes in the western mediterranean basin: from fuel-limited to drought-driven fire regime. Climatic change **110**(1), 215–226 (2012)

[16] Sil, Â., Fernandes, P.M., Rodrigues, A.P., Alonso, J.M., Honrado, J.P., Perera, A., Azevedo, J.C.: Farmland abandonment decreases the fire regulation capacity and the fire protection ecosystem service in mountain landscapes. Ecosystem Services **36**, 100908 (2019) https://doi.org/10.1016/j.ecoser.2019.100908

[17] Kreider, M.R., Higuera, P.E., Parks, S.A., Rice, W.L., White, N., Larson, A.J.: Fire suppression makes wildfires more severe and accentuates impacts of climate change and fuel accumulation. Nature Communications **15**, 2412 (2024) https://doi.org/10.1038/s41467-024-46702-0

[18] Malamud, B.D., Morein, G., Turcotte, D.L.: Forest fires: an example of self-organized critical behavior. Science **281**(5384), 1840–1842 (1998)

[19] Malamud, B.D., Turcotte, D.L.: Self-organized criticality applied to natural hazards. Natural Hazards **20**(2), 93–116 (1999)

[20] Giglio, L., Boschetti, L., Roy, D.P., Humber, M.L., Justice, C.O.: The collection 6 modis burned area mapping algorithm and product. Remote Sensing of Environment **217**, 72–85 (2018)

[21] Kelley, D.I., Burton, C., Di Giuseppe, F., Jones, M.W., Barbosa, M.L., Brambleby, E., McNorton, J.R., Liu, Z., Bradley, A.S., Blackford, K., *et al.*: State of wildfires 2024–2025. Earth System Science Data **17**(10), 5377–5488 (2025)

[22] Jones, M.W., Kelley, D.I., Burton, C.A., Di Giuseppe, F., Barbosa, M.L.F., Brambleby, E., Hartley, A.J., Lombardi, A., Mataveli, G., McNorton, J.R., *et al.*: State of wildfires 2023–2024. Earth System Science Data **16**(8), 3601–3685 (2024)

[23] San-Miguel-Ayanz, J., Schulte, E., Schmuck, G., Camia, A., Strobl, P., Liberta, G., Giovando, C., Boca, R., Sedano, F., Kempeneers, P., *et al.*: Comprehensive monitoring of wildfires in europe: the european forest fire information system (effis). Approaches to managing disaster-Assessing hazards, emergencies and disaster impacts **10**, 28441 (2012)

[24] García-Llamas, P., Suárez-Seoane, S., Taboada, A., Fernández-Manso, A., Quintano, C., Fernández-García, V., Fernández-Guisuraga, J.M., Marcos, E., Calvo, L.: Environmental drivers of fire severity in extreme fire events that affect mediterranean pine forest ecosystems. Forest Ecology and Management **433**, 24–32 (2019)

[25] Santoro, M., Cartus, O.: ESA Biomass Climate Change Initiative (Biomass_cci): Global Datasets of Forest Above-ground Biomass for the Years 2010, 2017 and 2018, V3. https://doi.org/10.5285/5f331c418e9f4935b8eb1b836f8a91b8 . Data set

[26] McNorton, J.R., Di Giuseppe, F.: A global fuel characteristic model and dataset for wildfire prediction. Biogeosciences **21**(1), 279–300 (2024)

[27] Richardson, D., Black, A.S., Irving, D., Matear, R.J., Monselesan, D.P., Risbey, J.S., Squire, D.T., Tozer, C.R.: Global increase in wildfire potential from compound fire weather and drought. npj Climate and Atmospheric Science **5**, 23 (2022) https://doi.org/10.1038/s41612-022-00248-4

[28] Lotka, A.J.: Elements of Physical Biology. Williams & Wilkins, Baltimore (1925)

[29] Volterra, V.: Variations and fluctuations of the number of individuals in animal species living together. ICES Journal of marine science **3**(1), 3–51 (1928)

[30] Clar, S., Drossel, B., Schwabl, F.: Forest fires and other examples of self-organized criticality. Journal of Physics: Condensed Matter **8**(37), 6803 (1996)

[31] Moritz, M.A., Morais, M.E., Summerell, L.A., Carlson, J., Doyle, J.: Wildfires, complexity, and highly optimized tolerance. Proceedings of the National Academy of Sciences **102**(50), 17912–17917 (2005)

[32] Calkin, D.E., Thompson, M.P., Finney, M.A.: Negative consequences of positive feedbacks in US wildfire management. Forest Ecosystems **2**(1), 9 (2015) https://doi.org/10.1186/s40663-015-0033-8 . Accessed 2026-02-10

[33] Pausas, J.G., Paula, S.: Fuel shapes the fire–climate relationship: evidence from mediterranean ecosystems. Global Ecology and Biogeography **21**(11), 1074–1082 (2012)

[34] Oliveras Menor, I., Prat-Guitart, N., Spadoni, G.L., Hsu, A., Fernandes, P.M., Puig-Gironès, R., Ascoli, D., Bilbao, B.A., Bacciu, V., Brotons, L., Carmenta, R., de-Miguel, S., Gonçalves, L.G., Humphrey, G., Ibarnegaray, V., Jones, M.W., Machado, M.S., Millán, A., Morais Falleiro, R., Mouillot, F., Pinto, C., Pons, P., Regos, A., Oliveira, M., Harrison, S.P., Armenteras Pascual, D.: Integrated fire management as an adaptation and mitigation strategy to altered fire regimes. Communications Earth & Environment **6**, 202 (2025) https://doi.org/10.1038/s43247-025-02165-9

[35] El Garroussi, S., Wetterhall, F., Barnard, C., Mazzetti, C., Lombardi, A., Di Giuseppe, F.: Optimized afforestation reduces flood risk and limits water loss in europe. Communications Sustainability **1**(1), 60 (2026)

[36] Uhlenbeck, G.E., Ornstein, L.S.: On the theory of the brownian motion. Physical review **36**(5), 823 (1930)

[37] Justus, C., Hargraves, W., Mikhail, A., Graber, D.: Methods for estimating wind speed frequency distributions. Journal of Applied Meteorology and Climatology **17**(3), 350–353 (1978)

[38] Bowden, G., Barker, P., Shestopal, V., Twidell, J.: The weibull distribution function and wind power statistics. Wind Engineering, 85–98 (1983)

Supplementary analysis

Tests for bimodality in the Iberia seasonal fire record

The two-component representation reduced AIC by 8.90 and BIC by 5.49 relative to a single Gaussian. Three of four diagnostics rejected Gaussianity at 5%; Jarque–Bera did not. These results support a two-mode descriptive model but do not independently establish a dynamical regime shift.

Table S1 Gaussian mixture comparison for annual total burned area across mainland Iberia, 2003–2025. Lower values indicate the preferred model.

Model	AIC	BIC
One Gaussian	418.54	420.81
Two Gaussians	409.64	415.32

Table S2 Tests of Gaussianity for annual total burned area. Anderson–Darling is reported as a decision at 5% because the workflow returns critical values.

Test	Statistic	p value	Gaussian at $\alpha = 0.05$
Shapiro–Wilk	0.823	0.00092	No
D'Agostino K^2	6.479	0.03918	No
Jarque–Bera	5.180	0.07502	Yes
Anderson–Darling	1.477	—	No

Independent evidence for the emergence of a two-mode fire season in Iberia

The MODIS burned-area record used in the main analysis covers only 2003–2025. We therefore use the longer national burned-area statistics for Spain and Portugal to test two aspects of the observational result: first, whether the MODIS record reproduces the interannual variability observed in an independent dataset; and second, whether the separation between ordinary and high-fire seasons is also present when a substantially longer period is considered.

The MODIS and EFFIS national datasets [23] differ in their spatial and temporal definitions. MODIS totals represent May–October burning over mainland Iberia, whereas the national statistics represent January–December totals for Spain and Portugal. Their absolute burned areas are therefore not expected to be identical. Nevertheless, over their common 2003–2024 period, the two records show very similar interannual variability (Fig. S1). Pearson correlation is $r = 0.979$ and Spearman rank correlation is $r = 0.967$, showing that years with relatively high or low burned area are consistently identified by the two datasets.

National totals are on average higher than the MODIS estimates, with an aggregate national-to-MODIS ratio of 1.22, consistent with differences in seasonal coverage, geographical domain and observation method. The close agreement in year-to-year variability provides an independent verification that the ordering of fire seasons identified from MODIS is robust.

The discrepancies in 2019, 2021 and especially 2023 are consistent with substantial burning outside the May–October observation window. In 2007, off-season burning contributes to the difference, but the inclusion of the Canary Islands in the

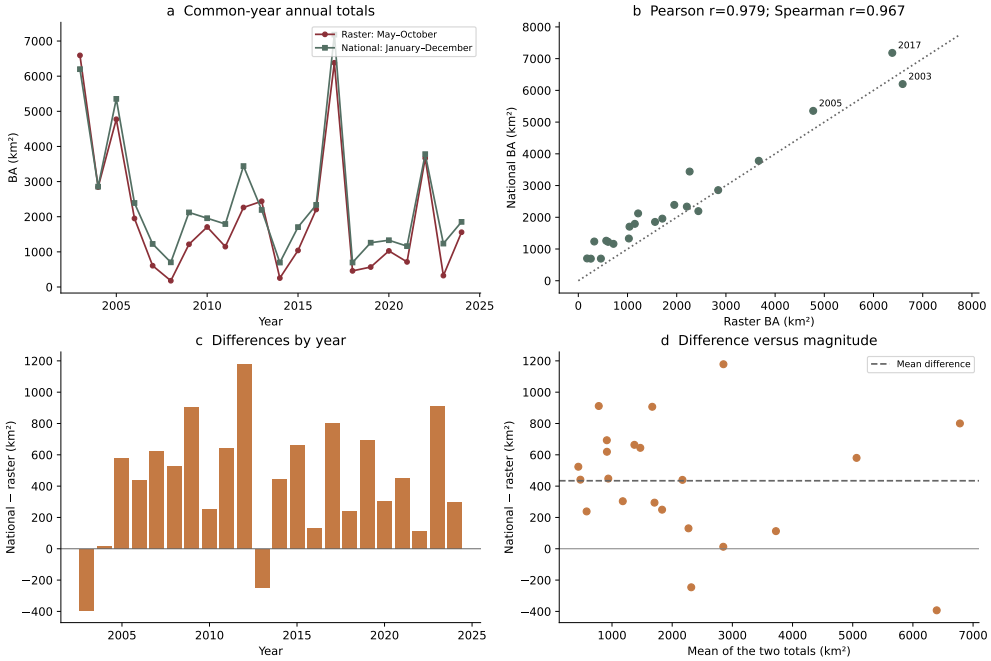


Fig. S1 Agreement between MODIS and independent national burned-area statistics. Comparison of annual burned area from the MODIS-based mainland Iberian record and the combined Spain–Portugal national statistics over their common 2003–2024 period. Despite differences in spatial coverage, seasonal definition and observation method, the two records exhibit closely matching interannual variability (Pearson $r = 0.979$; Spearman $r = 0.967$).

Spanish national statistics is also particularly important. We next repeated the distributional analysis independently for the two datasets. Over the common 2003–2024 period, fitting a two-component Gaussian mixture produces two density maxima in both the MODIS and national records (Fig. S2). Relative to a single Gaussian, the two-component representation is favoured for the MODIS record ($\Delta AIC = 6.60$, $\Delta BIC = 3.33$) and for the national statistics ($\Delta AIC = 8.48$, $\Delta BIC = 5.20$). Importantly, the same behaviour persists when the complete records are considered. For MODIS over 2003–2025, $\Delta AIC = 8.90$ and $\Delta BIC = 5.49$, while for the 45-year national record over 1980-2024 the corresponding values are 11.20 and 5.78. In all four fits, the fitted two-component density contains two local maxima. Thus, the separation identified in the MODIS record is reproduced by an independent observational record and is retained when the national time series is extended back to 1980.

The longer national record further allows us to examine when this distributional structure becomes apparent. Applying the same analysis to successive portions of the national time series shows that the separation between a dominant lower-burned-area group and a smaller group of high-burned-area seasons becomes increasingly evident from the 1990s onward (Fig. S3). The earlier 1980–2002 period provides substantially weaker evidence for two components ($\Delta AIC = 3.73$, $\Delta BIC = 0.33$), whereas the complete 1980–2024 record shows a clearer separation ($\Delta AIC = 11.20$, $\Delta BIC = 5.78$).

Table S3 Iberian burned-area totals derived from MODIS and reported by EFFIS for 2003–2024. MODIS values represent May–October totals over mainland Iberia, whereas EFFIS values represent full-year national totals for Portugal and Spain combined. All values are rounded to the nearest km^2.

Year	MODIS (km^2)	EFFIS (km^2)
2003	6,592	6,199
2004	2,843	2,856
2005	4,774	5,354
2006	1,951	2,391
2007	606	1,225
2008	178	702
2009	1,215	2,122
2010	1,708	1,957
2011	1,148	1,793
2012	2,263	3,441
2013	2,440	2,194
2014	254	695
2015	1,040	1,704
2016	2,206	2,336
2017	6,381	7,182
2018	459	697
2019	567	1,260
2020	1,027	1,331
2021	714	1,162
2022	3,668	3,780
2023	324	1,236
2024	1,559	1,854

The longer record therefore suggests that the two-group structure evident during the MODIS era was not equally pronounced throughout the entire observational period, but became more apparent during the later decades.

Additional statistical diagnostics support a departure from a simple Gaussian description of annual burned area, although they do not uniquely establish bimodality. Normality is rejected by most tests for both the MODIS and full national records, and fitting the same two-Gaussian representation across different record lengths produces a consistent high-fire/low-fire separation. However, alternative skewed single-peaked distributions can also provide competitive descriptions of these relatively short and strongly skewed records. We therefore interpret these analyses as evidence for a reproducible empirical two-group structure rather than as proof that the underlying burned-area distribution must be strictly bimodal.

Taken together, the three analyses provide complementary evidence for the observational framework used in the main text. MODIS reproduces the interannual ordering of an independent national record, the same two-component representation is recovered independently in both datasets, and the longer national record indicates that the

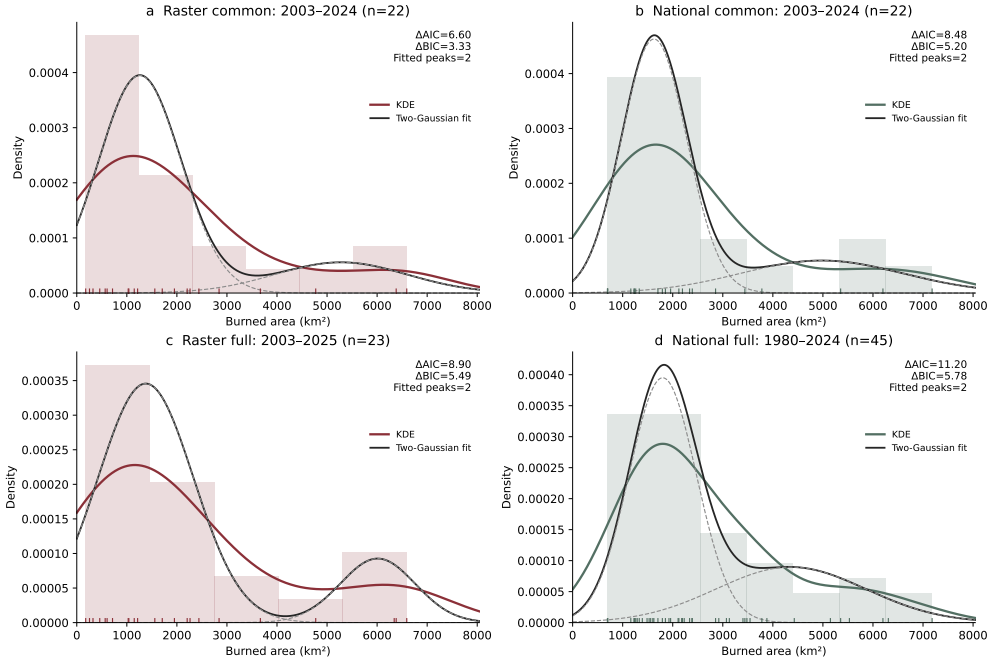


Fig. S2 Reproducibility of the two-component burned-area structure. Probability-density estimates and two-component Gaussian mixture fits for (a) MODIS over the common 2003–2024 period, (b) national Spain–Portugal statistics over the same period, (c) the complete MODIS record for 2003–2025, and (d) the complete national record for 1980–2024. Reported ΔAIC and ΔBIC values are relative to a single-Gaussian fit, such that positive values favour the two-component representation. Two maxima are present in each fitted mixture.

separation associated with recent high-fire seasons became more apparent during the later decades of the record.

5.5 Structural portability of the fire–fuel–suppression model to Greece

To test whether the annual burned-area behaviour reproduced for Iberia was specific to the regional calibration, or instead reflected a more general property of the model structure, we repeated the analysis for Greece using the same stochastic fire–fuel–suppression equations. Greece provides a useful contrast because its observed annual burned-area distribution is predominantly single-peaked rather than displaying the two-group structure identified in Iberia.

Annual burned area for Greece was calculated from the same MODIS Collection 6.1 burned-area product used in the Iberian analysis and aggregated over the full calendar year for 2003–2025. The Greek record is strongly skewed by a small number of large fire seasons, but the fitted two-component Gaussian mixture contains only one local density maximum (Fig. SXXb). We therefore interpret the observed Greek distribution as predominantly single-peaked, rather than as evidence of a distinct low- and high-fire structure.

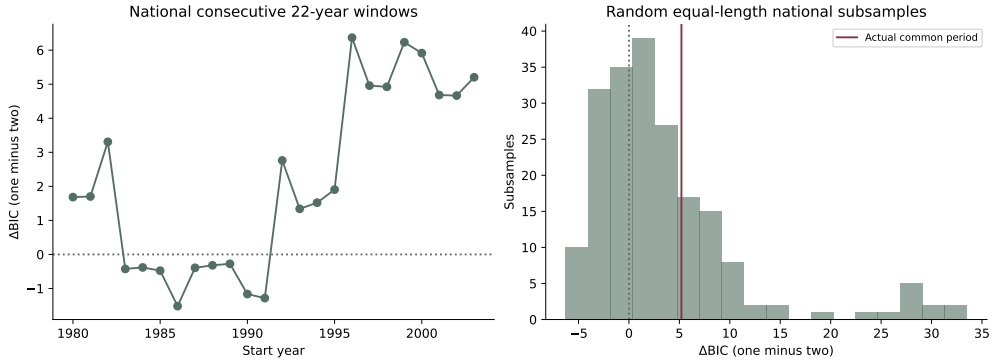


Fig. S3 Emergence of the high-fire component in the national record. Evolution of the fitted burned-area distribution through the longer Spain–Portugal national record. The early part of the record shows relatively weak separation between components, whereas a distinct high-burned-area group becomes increasingly apparent from the 1990s onward and persists through the recent period. The analysis is intended to identify when the empirical separation emerges in the record rather than to diagnose a discrete dynamical regime shift.

The model formulation was kept unchanged from the Iberian experiment. The ignition probability and magnitude, stochastic weather process, fuel-consumption coefficient, suppression-response timescale and numerical integration were all retained. Only the effective fuel-replenishment parameter, G, and the effective suppression parameter, c, were recalibrated against the observed Greek annual burned-area distribution.

Calibration minimized the first-order Wasserstein distance between observed and simulated annual burned-area fractions. To reduce sensitivity to individual stochastic realizations, the same independent weather and ignition realizations were used for all candidate parameter combinations during calibration. A differential-evolution search was used to identify the broad optimum, followed by a local grid refinement. Final evaluation used independent stochastic realizations that were not included in calibration.

The optimal Greek calibration was

$$G_{\mathrm{Greece}} = 3.17 \times 10^{-6}, \qquad c_{\mathrm{Greece}} = 0.0312,$$

compared with the Iberian reference values

$$G_{\mathrm{Iberia}} = 3.13 \times 10^{-6}, \qquad c_{\mathrm{Iberia}} = 0.04324.$$

This corresponds to

$$\frac{G_{\mathrm{Greece}}}{G_{\mathrm{Iberia}}} = 1.01, \qquad \frac{c_{\mathrm{Greece}}}{c_{\mathrm{Iberia}}} = 0.72.$$

The fitted effective fuel-replenishment parameter is therefore essentially unchanged between the two regions, whereas the fitted effective suppression parameter is approximately 28% lower in Greece. These quantities should be interpreted as effective parameters of the conceptual model rather than as direct measurements of vegetation productivity or firefighting capacity.

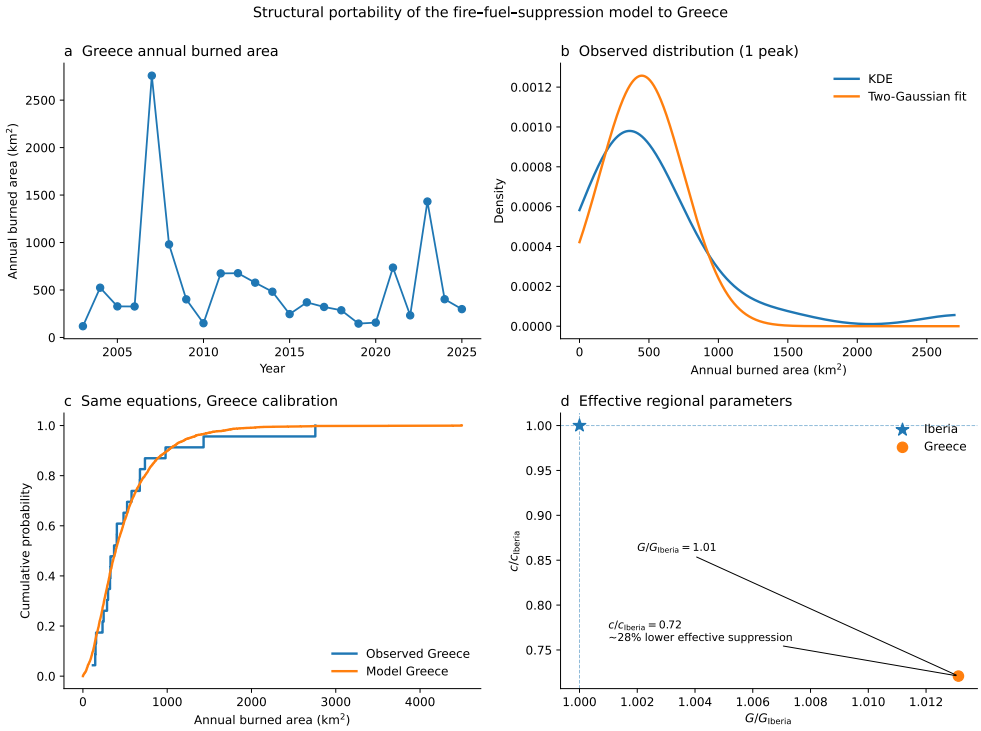


Fig. S4 Structural portability of the fire–fuel–suppression model to Greece. a, Annual burned area in Greece during 2003–2025. **b**, Observed annual burned-area distribution. Although a two-component Gaussian mixture provides a flexible representation of the skewed distribution, the fitted density contains only one local maximum. **c**, Empirical cumulative distributions of observed Greek annual burned area and independent simulations using the Greece-specific calibration. **d**, Calibrated Greek parameters relative to the Iberian reference. The effective fuel-replenishment parameter is nearly unchanged ($G/G_{\mathrm{Iberia}} = 1.01$), whereas the effective suppression parameter is lower ($c/c_{\mathrm{Iberia}} = 0.72$). Under these conditions the same model equations reproduce a predominantly single-peaked annual burned-area distribution rather than the two-group structure found for Iberia.

Independent simulations using the Greece-specific calibration reproduce the broad observed annual burned-area distribution. In particular, the empirical cumulative distribution of simulated burned area closely follows the observed distribution across most of its range (Fig. S4). At the same time, the fitted Greek distribution remains predominantly single-peaked, in contrast with the two-group behaviour reproduced for Iberia.

This comparison provides a test of the structural portability of the model. The same equations can reproduce qualitatively different annual burned-area regimes after adjustment of only two effective process parameters. The contrast between Greece and Iberia is particularly informative because the fitted fuel-replenishment parameters are nearly identical, whereas the effective suppression parameter differs substantially. Within the model, lower suppression allows fire to remove available fuel more frequently, reducing fuel retention and preventing the separation between low-fire and high-fire years that develops under the Iberian calibration. The Iberian two-group

structure is therefore not imposed by the model formulation, but emerges from the balance between fuel replenishment and suppression.

This experiment should not be interpreted as demonstrating parameter universality or as a predictive model for Greece. Rather, it shows that the same minimal dynamical framework can accommodate different regional fire regimes through changes in effective process strengths.